2022 Asia-Pacific Microwave Conference

Proceedings

Home

Program at a Glance

Author Index

Greetings from the Steering Committee Chair

Message From the Technical Program Committee Chair

2022 Asia-Pacific Microwave Conference Committee Officers

Copyright

Program at a Glance

Author Index

Organized and sponsored by

The Institute of Electronics Information and Communication Engineers (IEICE) of Japan

Supported by

Ministry of Internal Affairs and Communications

Special Collaboration with

Yokohama Convention & Visitors Bureau

Technical Sponsors

IEEE Microwave Theory and Technology Society (IEEE MTT-S)
IEEE Antennas and Propagation Society (IEEE AP-S)
European Microwave Association (EuMA)
Union Radio-Scientifique Internationale (URSI)
IEEE MTT-S Japan/Kansai/Nagoya Chapters
IEICE Technical Committee on Microwaves
IEICE Technical Committee on Electronics Simulation Technology
IEICE Technical Committee on Integrated Circuits and Devices
IEICE Technical Committee on Electron Devices
IEICE Technical Committee on Antennas and Propagation
IEICE Technical Committee on Electromagnetic Compatibility
IEICE Technical Committee on Wireless Power Transfer
IEICE Technical Committee on Microwave Photonics and Terahertz Photonic-Electronics Technologies
Japan Society of Electromagnetic Wave Energy Applications
Japan Institute of Electronics Packaging
IEEJ Investigating R&D Committee on Innovative Advanced Application Technology of Electromagnetic Waves in the 5G/Beyond 5G Era
IEEJ Technical Committee on Communications
IEEJ Research Committee on MBSE / MBD / Digital Twin for Communications
IEEJ Research Committee on ICT-based Smart Technologies and Their Social Implementation
IEEJ Research Committee on Communication Technologies Promoting Ubiquitous Work
IEEJ Investigating R&D Committee on High-frequency Magnetics
JSPS R024 Electromagnetic-Wave-Excited Reaction Field
JSPS University-Industry Cooperative Research Committee 187th committee on Metamaterials
Wireless Power Transfer Consortium for Practical Applications

Ministry of Internal Affairs and Communications

APMC 2022 Secretariat

For further information, please contact:
Prof. Yoshinori Kogami
[Chair, Steering Committee]
c/o Real Communications Corp.
3F Shinmatsudo S bldg., 1-409 Shinmatsudo,
Matsudo 270-0034, Japan
Phone: +81-47-309-3616,
Fax: +81-47-309-3617,
Email: mweapmc@io.ocn.ne.jp

APMC 2022 Secretariat
For further information, please contact:
Prof. Yoshinori Kogami
[Chair, Steering Committee]
c/o Real Communications Corp.
3F Shinmatsudo S bldg., 1-409 Shinmatsudo,
Matsudo 270-0034, Japan
Phone: +81-47-309-3616,
Fax: +81-47-309-3617,
Email: mweapmc@io.ocn.ne.jp

Virtual Interactive Forum

Interactive Forum A

IF-A01	Broadband SPST Switches in 250-nm GaN HEMT Process
	Yunshan Wang, Pragya Tripathi, Hoi-Wong Lei and Huei Wang (National Taiwan Univ., Taiwan)
IF-A02	A Reconfigurable 60-GHz VCO with -103.2 dBc/Hz Phase Noise in a 0.13-μm SiGe BiCMOS Technology
	Christian Hoyer, Florian Protze, Jens Wagner and Frank Ellinger (Technische Universität Dresden, Germany)
IF-A03	Self-Aligned On-Chip Spherical Dielectric Resonators and Antennas for SiGe MMIC
	Georg Sterzl (Univ. of Stuttgart, Germany); Yu Zhu (Technische Universität Dresden, Germany); Jan Hesselbarth (Univ. of Stuttgart, Germany); Corrado Carta and Marco Lisker (IHP, Germany); Frank Ellinger (Technische Universität Dresden, Germany)
IF-A04	Broadband Class-E Power Amplifier Design Employing a Double Reactance Compensation Matching Network
	Ziming Zhao and Xiao-Wei Zhu (Southeast Univ., China)
IF-A05	Harmonic Behavioral Model in RF Domain for Short-Wave Power Amplifier
	Tingting Yao, Jun Peng, Fei You and Songbai He (UESTC, China)
IF-A06	A 1.5-6 GHz Continuous Tuned GaAs MMIC Phase Shifter
	Xiao-Liang Wu, Jian-Bo Wang, Jian-Yu Ye and Guang Hua (Southeast Univ., China)
IF-A07	X-Band Filter-Amplifier for Radio Frequency Front-End Receiver Systems
	Phanam Pech, Samdy Saron, Girdhari Chaudhary and Yongchae Jeong (Jeonbuk National Univ., Korea)
IF-A08	A 3.5-GHz 6-Bit CMOS Vector-Summing Phase Shifter with Low Phase and Amplitude Errors Using Area-Resizing Technique
	Chia-Wei Hsu and Jia-Shiang Fu (NCU, Taiwan)
IF-A09	Vector Sum Phase Shifter Using Phase Control Linearization Technique
	Ren Imanishi and Hideyuki Nosaka (Ritsumeikan Univ., Japan)
IF-A10	A 28 GHz Complementary QVCO Using Current Re-Used and Parallel Coupling Technique
	Yu-Teng Chang (Yuan Ze Univ., Taiwan); Chin-Chia Chang and Hsin-Chia Lu (NTU, Taiwan)
IF-A11	A Novel Design Method of Class E/F Power Amplifier Based on Waveform Analysis
	Guoping Hong, Yonglun Luo, Rong Chang, Wanghong Yang and Danlei Xuan (UESTC, China)
IF-A12	A New Design for Class EF PA Based on Waveform Analysis
	Rong Chang, Yonglun Luo, Guoping Hong, Wanghong Yang and Danlei Xuan (UESTC, China)
IF-A13	2-18GHz Reconfigurable Distributed Power Amplifier Using 0.25um GaN Technology
	Xiaojing Hu, Zhuohao Liu and Ziqi Pu (UESTC, China); Pei-Ling Chi (NCTU,Taiwan); Xilin Zhang (UESTC, China); Xu Zhu and Xiang Li (Northern Institute of Electronic Equipment of China, China); Yong Wang and Tao Yang (UESTC, China, NCTU, Taiwan)
IF-A14	Inverse Class-F Linear PA for Middle Band 5G Applications
	Yuuri Honda, Satoshi Tanaka, Kenji Mukai, Yusuke Tanaka and Hiroshi Okabe (Murata Manufacturing Co., Ltd., Japan)
IF-A15	High-Power and Low-Loss Ku-Band GaN HEMT Switch with Inductive Resonator to Compensate for Off-Capacitance of HEMT
	Yoshifumi Kawamura, Tetsunari Saito, Kunihiro Endo, Masaomi Tsuru and Koji Yamanaka (Mitsubishi Electric Corp., Japan)
IF-A16	A CMOS Voltage-Controlled Oscillator Using Dual-Balance Capacitive-Division Structures
	Yu-Hsin Chang and Yong-Lun Luo (National Formosa Univ., Taiwan)
IF-A17	A Fixed-Frequency, Tunable Dielectric Resonator Oscillator with Phase-Locked Loop Stabilization
	Robin Kaesbach, Marcel van Delden and Thomas Musch (Ruhr-Universität Bochum, Germany)
IF-A18	28 GHz Band Wireless Power Transfer Experiments with a GaAs Rectenna MMIC with an Inductive High Impedance Patch Antenna
	Tsukasa Hirai, Takumi Itoh, Yuya Hirose, Naoki Sakai, Keisuke Noguchi and Kenji Itoh (Kanazawa Inst. of Tech., Japan); Naoki Hasegawa, Takashi Hirakawa, Yuta Nakamoto and Yoshichika Ohta (Softbank Corp., Japan)
IF-A19	5.8 GHz Band High Power Rectenna with a Monopole Antenna on an Artificial Magnetic Conductor
	Naoki Furutani, Keisuke Miyashita, Shigeru Makino, Fumiya Komatsu, Naoki Sakai and Kenji Itoh (Kanazawa Inst. of Tech., Japan)
IF-A20	Analysis of the Operation of a Hybrid Amplifier Based on the Doherty Amplifier
	Ren Furumoto, Daisuke Yasunobu and Kenjiro Nishikawa (Kagoshima Univ., Japan)

X-band Filter-Amplifier for Radio Frequency Front-End Receiver Systems

Phanam Pech #1, Samdy Saron #2, Girdhari Chaudhary *3, and Yongchae Jeong #4

#Division of Electronics and Information Engineering, Jeonbuk National University
Jeollabuk-do, Republic of Korea
1pechphanam@jbnu.ac.kr
2saronsamdy@jbnu.ac.kr
4ycjeong@jbnu.ac.kr
*JIANT-IT Human Resource Development Center, Jeonbuk National University
Jeollabuk-do, Republic of Korea
3girdharic@jbnu.ac.kr

***Abstract* — This paper presents an integrated design of substrate integrated waveguide (SIW) bandpass filter (BPF) with a discrete low noise amplifier (DLNA). The SIW BPF was designed to match the complex source impedance of the low noise transistor (LNTR) and acted as the input matching network (IMN). For validation, a DLNA was designed for X-band application with the center frequency (f_0) of 10 GHz. At f_0, the measured small-signal gain and noise figure of the proposed DLNA with SIW BPF IMN are 12.85 dB and 2.15 dB, respectively. The proposed DLNA provides high out-of-band signal suppression.**

Index Terms — bandpass filter, low noise amplifier, subsrtate integrated waveguide.

I. Introduction

Low noise amplifiers (LNAs), and bandpass filters (BPFs) are essential components in radio frequency (RF) front-end receiver systems. The LNA is generally used to enhance the power of the RF receiving signal with minimizing noise as small as possible, and it is usually cascaded with BPFs for harmonics rejection or frequency selection [1]-[2]. Typically, the BPFs and LNAs are designed individually with a system impedance that is usually 50 Ω. With the increasing demand for wireless communication systems, the integration designs of BPFs with LNAs were investigated in the literatures. To fulfill this requirement, the BPFs were designed to match the arbitrary real and/or complex termination impedances and acted as the matching networks (MNs). In [3]-[4], the designs of BPF MN based on the coupling matrix technique were realized using coupled waveguide cavities, while the bias circuits and transistor connection pads were realized on microstrip lines (MLs). Similarly, the integration designs of BPF with amplifier using substrate integrated waveguide (SIW) MNs were presented in [5]-[6]. In [5], the design method was based on active coupling matrix. In [6], a power amplifier (PA) was designed with SIW BPF output MN (OMN). Its electrical performances were compared to the electrical performances of conventional BPF cascaded with conventional PA which were designed separately with the termination impedance of 50 Ω. By using the integration design method, better electrical performances with smaller circuit sizes could be obtained.

In this paper, an integration design of DLNA with BPF IMN is presented. The design parameters of the proposed BPF IMN can be obtained easily by using admittance inverters cascaded with LC-resonators. The proposed BPF IMN is realized from SIW cavities. By using the integration design DLNA with SIW BPF IMN, a good frequency selectivity with high out-of-band signal suppression is obtained.

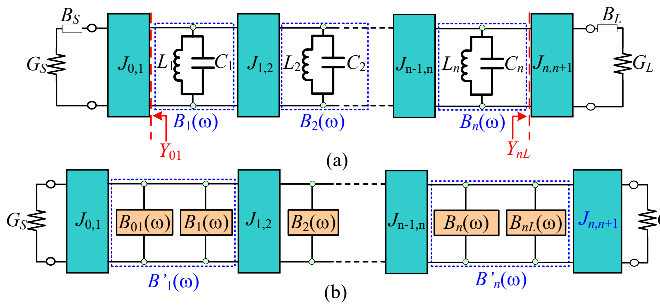

Fig. 1. Structure of arbitrary termination impedances BPF: (a) J-inverters with LC-resonators and (b) its equivalent structure.

II. Design Methods

The structures of arbitrary termination impedances (ATI) BPF is presented in Fig. 1. The source and load admittances are $Y_S = G_S \pm jB_S$ and $Y_L = G_L \pm jB_L$, respectively. Typically, $Y_S = 1/Z_S$ and $Y_L = 1/Z_L$ where $Z_S = R_S \pm jX_S$ and $Z_L = R_L \pm jX_L$. The complex admittances cannot directly match the adjacent J-inverters. Therefore, the admittances Y_{01} and Y_{nL} are still in complex forms. According to the structure in Fig. 1(a), $Y_{01} = G_{01} \pm jB_{01} = J^2_{01}/Y_S = J^2_{01}(R_S \pm jX_S)$ and $Y_{nL} = G_{nL} \pm jB_{nL} = J^2_{nL}/Y_L = J^2_{n,n+1}(R_L \pm jX_L)$ can be obtained. The susceptances of Y_{01} and Y_{nL} are combined with the susceptances of the first and the last LC-resonators, respectively, as shown in Fig. 1(b). The new susceptances, $jB'_1(\omega) = jB_{01}(\omega) + jB_1(\omega)$ is used to calculate the slope parameter for the first LC-resonator while $jB'_n(\omega) = jB_n(\omega) + jB_{nL}(\omega)$ is used to calculate the slope parameter for the last LC-resonator. To match the imaginary parts of termination admittances, the resonant frequencies of the first and the last resonators must be detuned and can be calculated from (1) [7].

$$f_{S1,nL} = f_0\left[\sqrt{1+\left(\frac{G_{S,L}\mathrm{FBW}}{2B_{S,L}g_{0,n}g_{1,n+1}}\right)^2}+\frac{G_{S,L}\mathrm{FBW}}{2B_{S,L}g_{0,n}g_{1,n+1}}\right], \quad (1)$$

where f_{S1} and f_{nL} are the new resonant frequencies of the first and the last resonators, respectively; g_0, g_1, g_n, and g_{n+1} are the element values of the low-pass prototype. The intermediate

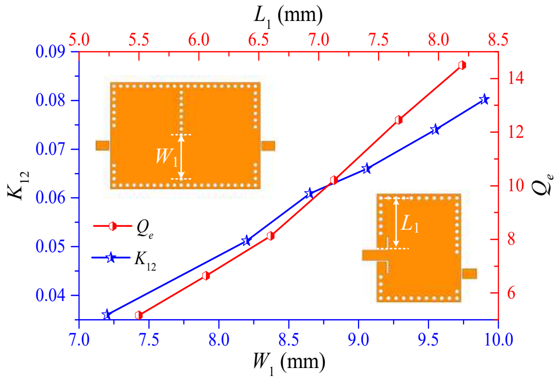

Fig. 2. Extracted $Q_{eS,eL}$ and K_{12} of SIW cavities: K_{12} versus W_1 and $Q_{eS,eL}$ versus L_1.

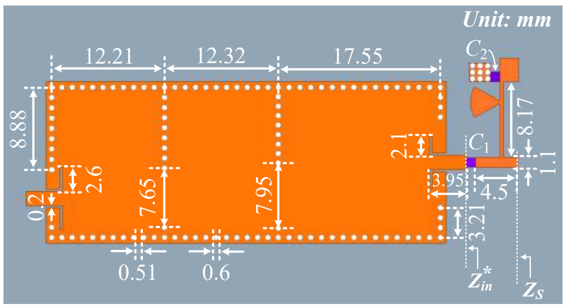

Fig. 3. Layout with dimension of proposed SIW BPF IMN.

resonators are not affected by complex impedance. When the imaginary parts of Z_S and Z_L are zeros, $f_{S1} = f_{nL} = f_0$ is obtained.

By arbitrarily choosing inductor L_i (i = 1, 2, 3, ⋯, n-1), the capacitance of the parallel resonator can be obtained from $C_i = 1/\omega^2 L_i$. The slope parameters of the first, intermediate, and last resonators can be found with $b_1 = 2\pi f_{S1}$, $b_{i+1} = 2\pi f_0$, and $b_n = 2\pi f_{nL}$, respectively. The values of J-inverters cab be calculated from the following equations.

$$J_{01} = \sqrt{\frac{G_S \mathrm{FBW} b_1}{g_0 g_1}}, \quad J_{i,i+1} = \mathrm{FBW}\sqrt{\frac{b_i b_{i+1}}{g_i g_{i+1}}}, \quad J_{n,n+1} = \sqrt{\frac{G_L \mathrm{FBW} b_n}{g_n g_{n+1}}}, \quad (2)$$

where FBW is the fractional bandwidth of the BPF. The coupling coefficient ($K_{i,i+1}$) of the resonator and the external quality factors ($Q_{eS,Ln}$) can be defined as follows [2].

$$K_{i,i+1} = \frac{J_{i,i+1}}{\sqrt{b_i b_{i+1}}}, \quad Q_{S1} = \frac{G_S b_1}{J_{01}^2}, \quad Q_{Ln} = \frac{G_L b_n}{J_{n,n+1}^2}, \quad (3)$$

Further, $Q_{eS,Ln}$ and $K_{i,i+1}$ can be extracted from electromagnetic (EM) simulation by using the following equations.

$$K_{i,i+1} = \pm\frac{f_H^2 - f_L^2}{f_H^2 + f_L^2}, \qquad Q_{eS\_EM,eL\_EM} = \frac{f_{S1,Ln}}{\Delta f_{\pm 3\mathrm{dB}}}, \quad (4)$$

where $\Delta f_{\pm 3\mathrm{dB}}$ is the 3 dB-bandwidth while f_H and f_L are denoted the higher and lower resonant frequencies, respectively.

Fig. 2 shows the extracted $Q_{eS,Ln}$ and $K_{i,i+1}$ from SIW cavities. The $Q_{eS,eL}$ can be controlled by moving the tap position from the short-circuit of the via-hole. The $Q_{eS,eL}$ is decreased as the tap position from via-hole (L_1) increases. Similarly, the value of K_{12} has increased as the width of the iris window (W_1) increases. The BW of the SIW BPF can be controlled by adjusting the coupling iris window.

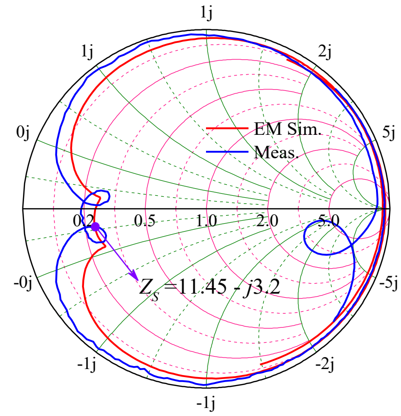

(a)

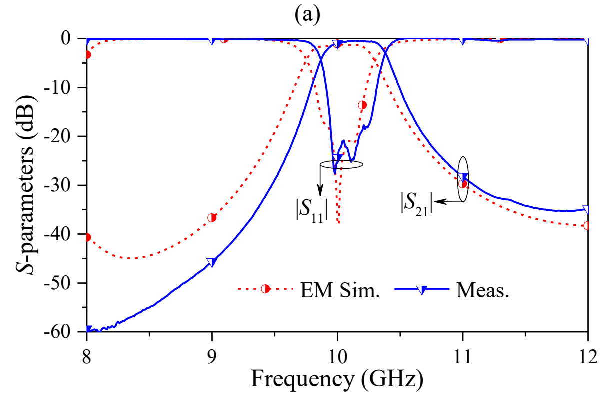

(b)

Fig. 4. The comparison between EM simulation and measurement results: (a) impedance points on Smith chart and (b) S-parameters.

III. Integrated Design of DLNA with SIW BPF IMN

For experimental validation, the proposed DLNA with SIW BPF IMN was designed by using NE32684A LNTR from NEC. Under the bias conditions of V_{GS} = –0.325 V and V_{DS} = 2 V, Z_S = 11.45 – j3.2 Ω and Z_L = 17.24 – j14 Ω were extracted at f_0. Z_S was transformed to Z_{in} by the bias circuit and a dc-block. From electrical simulation with ADS software, Z_{in} = 15 - j25 Ω was obtained. The BPF IMN was designed with FBW, resonator order (n), and input return loss ($|S_{11}|$) of 5%, 3, and 20 dB, respectively, with Chebyshev response. From (1), f_{nL} was calculated and detuned to 10.5 GHz. By choosing L_i = 2 nH, C_1 = C_i = 1.2665 pF and C_n = 1.1487 pF were calculated. Similarly, J_{01} = 0.003053, J_{12} = 0.000409, J_{23} = 0.000433, and J_{34} = 0.00544 were calculated by using (2). $K_{12} = K_{23}$ = 0.05151 while Q_{eS} = 17 and Q_{eL} = 17.12 were calculated from (3). The output MN (OMN) was realized using MLs.

IV. Simulation and Measurement Results

The proposed DLNA was implemented on RT/Duriod 5880 substrate with ε_r = 2.2 and h = 0.508 mm. The layout with dimensions of proposed SIW BPF IMN was shown in Fig. 3. The matching impedances and S-parameter responses obtained from EM simulation and measurement results are shown in Fig. 4(a) and (b), respectively. The target impedance of Z_S was obtained at f_0 with the measured insertion loss of 0.96 dB.

Photograph of the fabricated DLNA with SIW BPF IMN was shown in Fig. 5. Fig. 6 shows the comparison of

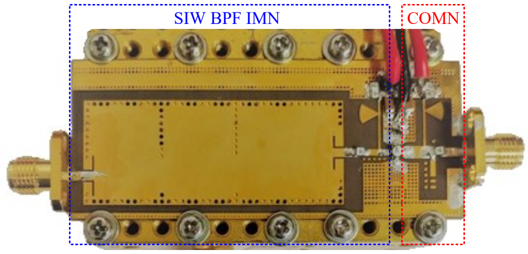

Fig. 5. Photograph of fabricated DLNA.

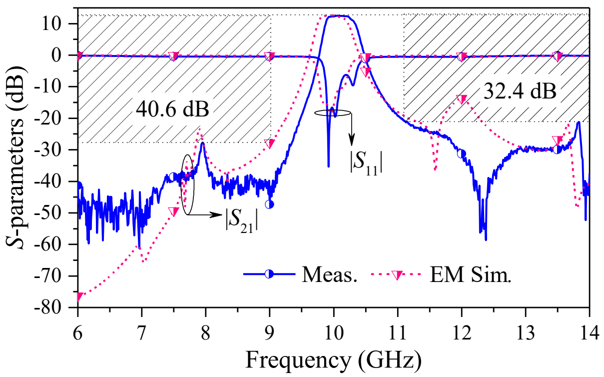

Fig. 6. The comparison of *S*-parameters between EM simulation and measurement results.

S-parameters obtained from EM simulation and measurement within the frequency range from 6 to 14 GHz. The measured *S*-parameter response of proposed DLNA was shifted up compared to the response obtained from EM simulation. The small-signal gain of 12.85 dB was obtained at f_0. The minimum attenuation of 40.6 dB and 32.4 dB were obtained from 6 to 9.1 GHz and 11.2 to 14 GHz, respectively. Fig. 7 shows the comparison of noise figure (NF) between EM simulation and measurement results. At f_0, the measured NF is 2.15 dB. For the output power test, the continuous-wave (CW) signal was used in the measurement. The output power at 1-dB compression point (P_{1dB}) of 8.07 dBm was measured at f_0 and it was denoted in Fig. 8. Similarly, the measured input third-order intercept point (IIP3) is approximately 14.2 dBm while the output third-order intercept point (OIP3) is around 26 dBm. The proposed DLNA with SIW BPF IMN was design and implemented on a simple ML at *X*-band, which is a simple and cheap fabrication process.

V. Conclusion

This paper demonstrates a design approach of an integrated design between SIW BPF and DLNA. For experimental demonstration, the proposed DLNA with SIW BPF IMN was fabricated and measured. The measured frequency response of proposed DLNA was shifted up compared to the responses obtained from EM simulation due to the slightly different during the fabrication process. However, the proposed DLNA provides good out-of-band signal suppression at the stopbands. The proposed DLNA can remove a receiving BPF cascaded from the receiving antennas and also reduce the complexity of the receiver in the RF front-end systems. With the obtained electrical performances, the proposed DLNA design method can be applied to RF circuits and RF front-end systems designs.

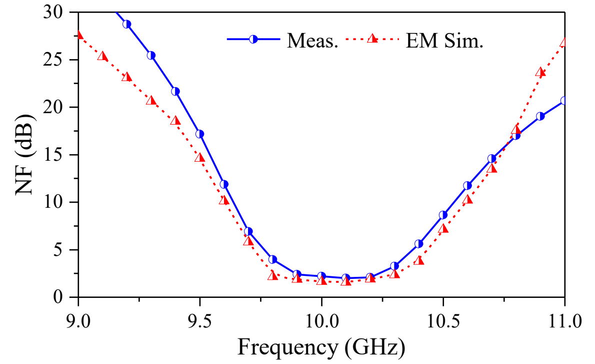

Fig. 7. The comparison of noise figures between EM simulation and measurement results.

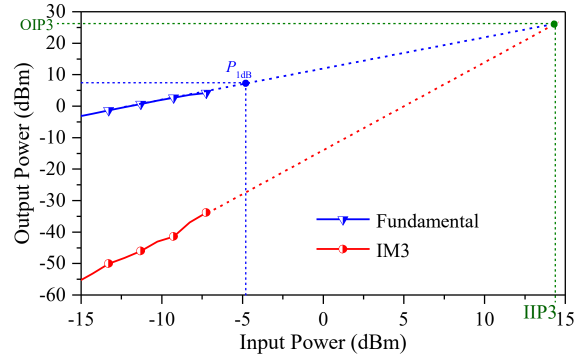

Fig. 8. Measured IIP3 and OIP3 of proposed DLNA.

Acknowledgement

This research was supported by National Research Foundation of Korea (NRF) grant funded by Korean Government (MSIT) under grant 2020R1A2C2012057 and in part by Basic Science Research Program through the NRF of Korea, funded by Ministry of Education under grant under grant 2019R1A6A1A0903171.

References

[1] B. Razavi, *RF Microelectronics*, 2nd Edition, pp. 157-250, Pearson Education, Inc., 2012.

[2] G. L. Matthaei, L. Yong, and E. M. T. Jones, *Microwave Filter, Impedance-Matching Networks, and Coupling Structures*, New York, NY, USA: McGraw-Hill, 1964.

[3] Y. Goa, J. Powell, X. Shang, and M. J. Lancaster, "Coupling matrix-based design of waveguide filter amplifiers," *IEEE Trans. Microwave Theory & Tech.*, vol. 66, no. 12, pp. 5300-5309, Dec. 2018.

[4] Y. Goa, X. Shang, C. Guo, J. Powell, Y. Wang, and M. J. Lancaster, "Integrated waveguide filter amplifier using the coupling matrix technique," *IEEE Microw. Wireless Compon. Lett.*, vol. 29 no. 4, pp. 267-269, Apr. 2019.

[5] Y. Goa, F. Zhang, X. Lv, C. Guo, X. Shang, L. Li, J. Liu, Y. Liu, Y. Wang, and M. J. Lancaster, "Substrate integrated waveguide filter-amplifier design using active coupling matrix technique," *IEEE Trans. Microwave Theory & Tech.*, vol. 68, no. 5, pp. 1706-1716, May 2020.

[6] P. Pech, P. Kim, and Y. Jeong, "Microwave amplifier with substrate integrated waveguide bandpass filter matching network," *IEEE Microw. Wireless Compon. Lett.*, vol. 31 no. 4, pp. 401-404, Apr. 2021.

[7] D. Swanson, and G. Macchiarella, "Microwave filter design by synthesis and optimization," *IEEE Microw. Mag.*, vol. 8 no. 2, pp. 55-69, Apr. 2007.